Multifidelity Optimization Under Uncertainty for a Tailless Aircraft

Anirban Chaudhuri*[1], John Jasa†[2], Joaquim R. R. A. Martins‡[2], and Karen Willcox§[1]
[1]*Massachusetts Institute of Technology, Cambridge, MA, 02139, USA*
[2]*University of Michigan, Ann Arbor, MI, 48109, USA*

This paper presents a multifidelity method for optimization under uncertainty for aerospace problems. In this work, the effectiveness of the method is demonstrated for the robust optimization of a tailless aircraft that is based on the Boeing Insitu ScanEagle. Aircraft design is often affected by uncertainties in manufacturing and operating conditions. Accounting for uncertainties during optimization ensures a robust design that is more likely to meet performance requirements. Designing robust systems can be computationally prohibitive due to the numerous evaluations of expensive-to-evaluate high-fidelity numerical models required to estimate system-level statistics at each optimization iteration. This work uses a multifidelity Monte Carlo approach to estimate the mean and the variance of the system outputs for robust optimization. The method uses control variates to exploit multiple fidelities and optimally allocates resources to different fidelities to minimize the variance in the estimates for a given budget. The results for the ScanEagle application show that the proposed multifidelity method achieves substantial speed-ups as compared to a regular Monte-Carlo-based robust optimization.

I. Introduction

Uncertainties exist in most engineering systems and accounting for these uncertainties during the design process is key to obtaining robust systems that satisfy performance requirements under varying conditions. In contrast with deterministic optimization, where commonly safety factors are used to get a conservative design, optimization under uncertainty (OUU) seeks efficient designs that are likely to meet performance requirements under varying conditions. In OUU, statistics of quantities of interest need to be estimated at many points in the design space, which is usually done using Monte Carlo methods that require large number of high-fidelity model evaluations to meet accuracy requirements. Figure 1a. shows a representation of OUU, where Monte Carlo estimates (inner-loop) for the output statistics are evaluated in each optimization iteration (outer-loop) using a single high-fidelity model. If the high-fidelity model is expensive then the cost of OUU becomes intractable. Thus, although OUU offers a probabilistic framework that leads to flexibility in treatment of uncertainty in the system, it is computationally prohibitive to implement in most engineering applications desiring a certain level of accuracy.

One way to reduce the computational cost of OUU is by using cheap-to-evaluate low-fidelity models to speed up the estimators with occasional recourse to the expensive high-fidelity model to ensure unbiasedness [1–3]. Figure 1b shows a framework for multifidelity OUU. Low-fidelity models are approximations for the high-fidelity models that can provide the general trend of the outputs to a certain extent. They can be data-fit surrogate models, approximations of underlying physics, or reduced-order models. More details about different types of low-fidelity models used in multifidelity methods can be found in [4].

There have been various efforts for developing multifidelity methods for optimization and uncertainty quantification and a survey of such methods can be found in [4]. For optimization, bifidelity approaches have been developed that use data-fit Gaussian process surrogates with adaptive sampling for occasional queries to the high-fidelity model to do Bayesian optimization [5, 6]. There are recent extensions of Bayesian optimization that combine multiple (≥ 2) fidelities [7, 8] to achieve faster convergence. Similarly, there have been efforts on developing multifidelity methods for uncertainty quantification using Bayesian regression [9], polynomial chaos expansions, and stochastic collocation methods [10]. Multifidelity uncertainty quantification methods based on Monte Carlo simulation generally combine multiple fidelities using control variates [11] for obtaining a lower variance in the multifidelity estimator compared to

*Postdoctoral Associate, Department of Aeronautics and Astronautics, anirbanc@mit.edu, AIAA member.
†Graduate Research Assistant, Department of Aerospace Engineering, johnjasa@umich.edu, AIAA student member.
‡Professor, Department of Aerospace Engineering, jrram@umich.edu, AIAA Fellow.
§Professor, Department of Aeronautics and Astronautics, kwillcox@mit.edu, AIAA Associate Fellow.

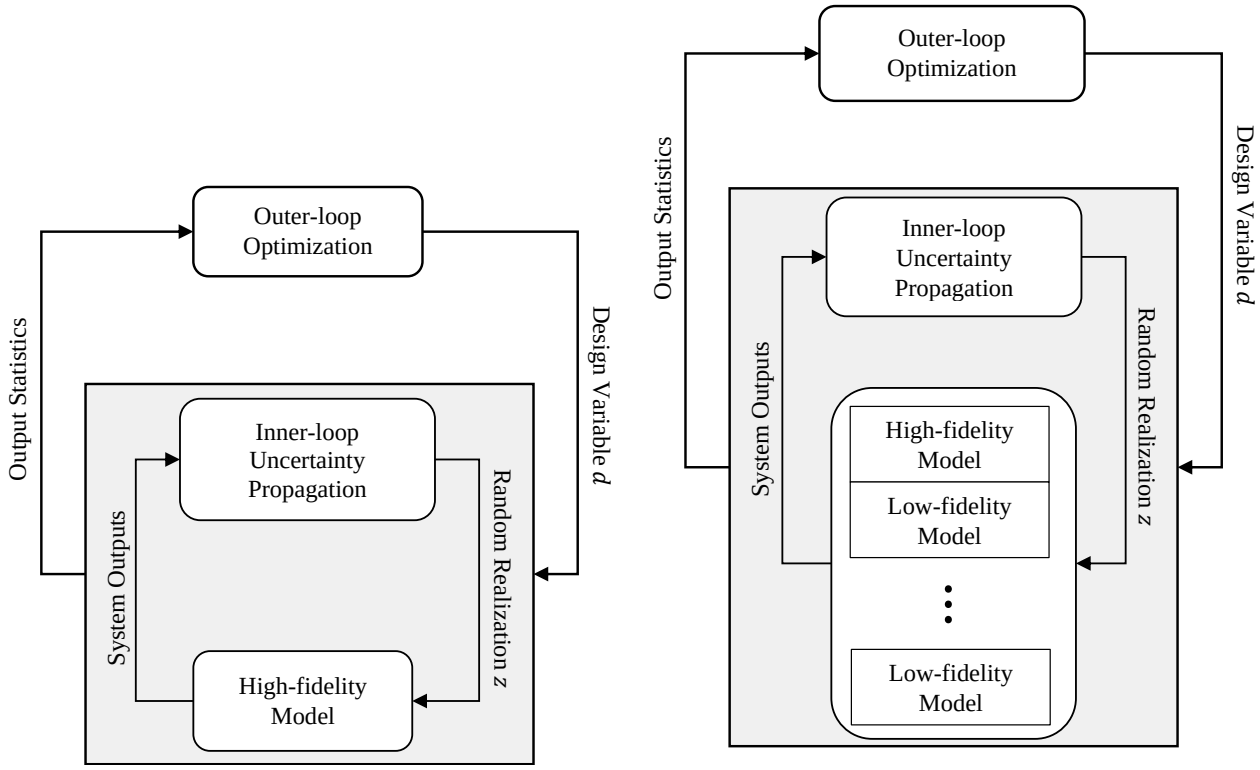

(a) Single high-fidelity model

(b) Multiple fidelity models

Fig. 1 Optimization under uncertainty using a single high-fidelity model, or multiple fidelities.

the single-fidelity Monte Carlo estimator at the same cost. The multilevel Monte Carlo [12] method uses the known complexity of the different models to construct the control variates. The StackMC approach [13] uses data-fit surrogate models and cross-validation to implement a control variates method for variance reduction.

In this work, we use the control-variates-based multifidelity Monte Carlo (MFMC) method to estimate the statistics for OUU. MFMC combines information from multiple (≥ 2) fidelities to reduce the overall error in the estimates. The MFMC method for estimating mean is described in [14] and is applicable to any type of low-fidelity model. The MFMC method for estimating the variance has been used for global sensitivity analysis [15]. The MFMC method optimally allocates resources between different models in order to minimize the error in the estimate for a given computational budget. Here, we present a multifidelity method for robust optimization using MFMC for estimating the mean and the variance. A bifidelity implementation of MFMC with separate set of samples for the mean and the variance estimates has been used for robust optimization in [3]. In this work, we extend the MFMC method for multiple fidelities in robust optimization and find the optimal allocation of resources to minimize the error in the mean and variance estimates using the same set of samples. The approach maintains the same level of accuracy as a regular Monte Carlo estimate using high-fidelity solves (Figure 1a), while needing substantially less computational effort.

We demonstrate the proposed multifidelity method for a tailless aircraft design. Specifically, we aim to find a robust tailless aircraft design that is protected against the risks from the uncertainties in flight conditions and manufacturing. Tailless aircraft offer aerodynamic and environmental benefits at reduced direct operating costs. They can be small-scale, like micro UAVs, or very large scale, like the blended-wing-body design [16]. In this paper, we study a model based on the Boeing Insitu ScanEagle because it has a variety of uses in both the civilian and military realms. The ScanEagle UAV was originally developed to fly missions to track schools of tuna, but it was later developed as a general and modular platform often used for military purposes as well. It is used for reconnaissance, person-of-interest tracking, and ordinance delivery missions, and at any given time there are an average of 17 ScanEagle aircraft in flight globally [17]. It can be launched from a ship or on ground from a unique launching and retrieval system, allowing it to operate in many varied conditions. Fig. 2 shows the ScanEagle aircraft.

Tailless aircraft like the ScanEagle are challenging to design because they involve a tightly coupled multidisciplinary

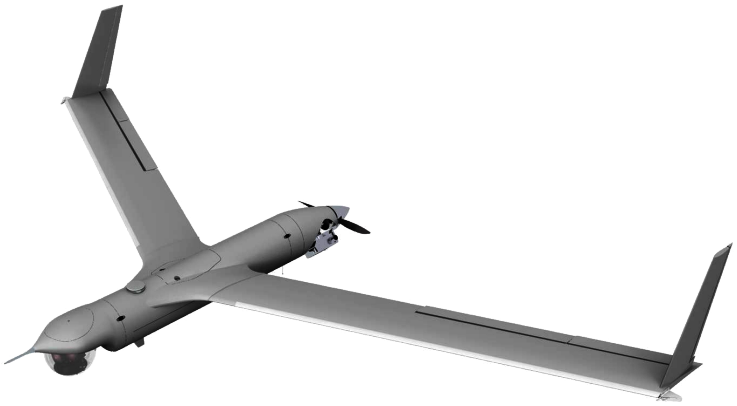

Fig. 2 ScanEagle aircraft with baseline configuration (image used with permission from Rohr 3D Solutions, LLC).

system and their unconventional configuration makes stability considerations more critical. The coupling effects between disciplines create design trade-offs and complicates the process of finding good aircraft designs. An experienced aircraft designer may be able to consider some of these interdisciplinary tradeoffs, but there are more than dozens of coupled disciplines. Aerodynamics, structures, propulsion, controls, thermal effects, internal electronics packing, and trajectory are just some of these disciplines. In this work, we use a multidisciplinary feedback-coupled model with exchange of information between the aerodynamic analysis and the structural analysis.

We can evaluate and optimize a design using multidisciplinary design optimization (MDO) to consider the trade-offs between disciplines. MDO has been widely used for aircraft to evaluate conventional and new designs while considering many different disciplines [18–21]. However, aircraft operate at uncertain conditions. For example, wind gusts may affect the apparent air speed over a wing, or engine performance might be degraded due to weather or air quality. Additionally, there are also manufacturing uncertainties like uncertainty in material properties, manufacturing tolerances, etc. The lift-producing wing in the tailless aircraft is even more important for control than a conventional design, which means that it is especially important to account for these uncertainties and the resulting risks in the design process. We treat the ScanEagle model as black-box and the proposed multifidelity method is not restricted to any particular choice of low-fidelity models.

The remainder of the paper is organized as follows. Section II describes the computational model for the ScanEagle tailless aircraft and the optimization problem formulation. The multifidelity robust optimization method using MFMC is described in Section III followed by the results for the ScanEagle aircraft in Section IV. Section V presents the conclusions.

II. Problem Setup

The first part of this section describes the computational model used for analyzing the ScanEagle tailless aircraft followed by the optimization problem formulation used in this work.

A. Computational Model

To model this aircraft we use OpenAeroStruct, an open-source aerostructural analysis and optimization tool [22]. OpenAeroStruct combines a vortex lattice method and 1-D finite-element analysis to model lifting surfaces, such as aircraft wings and tails. OpenAeroStruct has been developed in NASA's OpenMDAO framework [23] which streamlines the model development and interdisciplinary communication. Once an aircraft model is set up in OpenAeroStruct, users can select from a range of discretizations to control the level of fidelity of the analysis. OpenAeroStruct includes visualization tools to view optimization progress and the designs at each iteration. Figure 3 shows an example of analysis for a baseline ScanEagle model in OpenAeroStruct. Table 1 details the nominal parameters for ScanEagle used in this study.

OpenAeroStruct uses a 2-D vortex lattice method to perform the aerodynamic analysis. This method can be thought of as an extension of lifting-line theory, but is more general in that it can model low aspect ratio wings, swept wings,

Table 1 Nominal ScanEagle parameters used in the computational model.

Parameter	Value	Units
MTOW	22	kg
OEW	10	kg
Cruise speed	22.9	m/s
Cruise altitude	4.57	km
Range	1800	km
Wingspan	3.11	m
Wing sweep	20	degrees
Root chord	0.3	m
Spar Young's modulus	85	GPa
Spar Shear modulus	25	GPa
Spar yield	350	MPa
Spar density	1600	kg/m^3

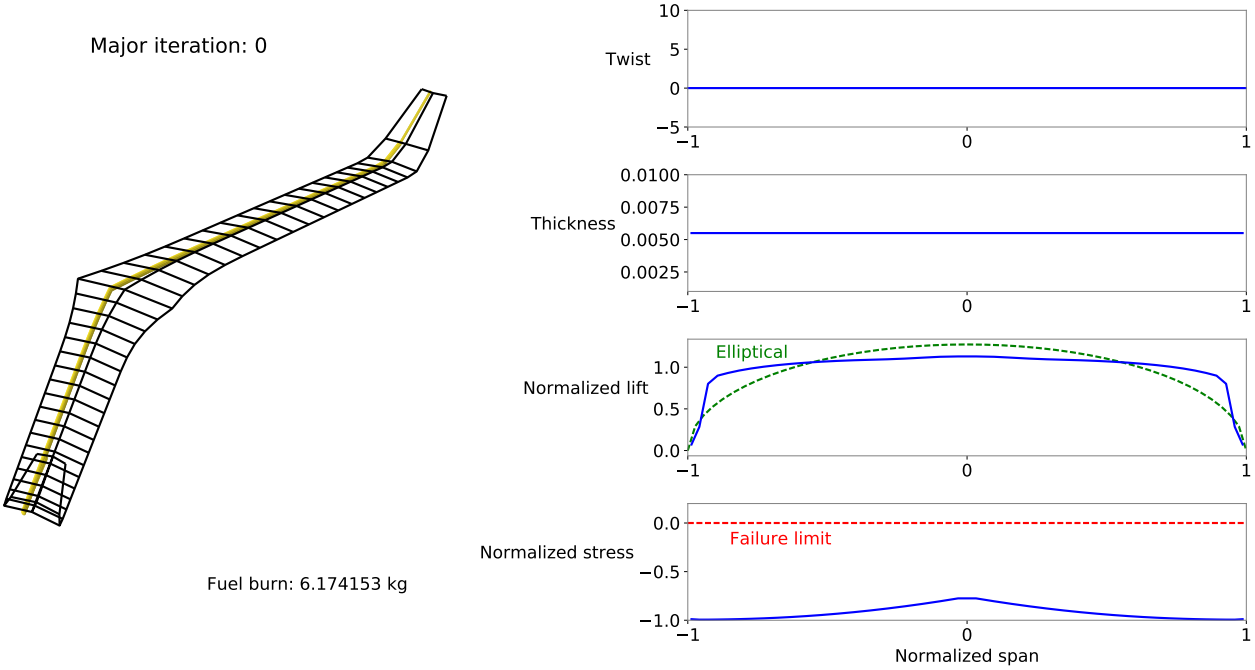

Fig. 3 Analysis of baseline ScanEagle model using OpenAeroStruct.

delta wings, and cambered airfoils more accurately. To compute the aerodynamic forces acting on a lifting surface, we construct a series of horseshoe vortices based on the planform shape. We then enforce the condition that the normal flow velocity must be zero at collocation points on the lifting surface, which allows us to solve for the vortex circulations, and thus the aerodynamic forces.

For the structural analysis, OpenAeroStruct uses a 1-D series of 6-degree-of-freedom beam elements connected end-to-end to represent the wing structural spar. We construct the global stiffness matrix for the spar and compute the nodal displacements and rotations based on the forces and moments acting on the lifting surface. The wingbox structural properties are represented by an equivalent tubular cross-section to simplify the analysis and parameterization.

These aerodynamic and structural analyses are coupled within OpenAeroStruct using a consistent and conservative transfer scheme. Because OpenAeroStruct is implemented in OpenMDAO, a variety of solvers can be used to converge this coupled aerostructural system, including block Gauss–Seidel or Newton for the nonlinear system. OpenAeroStruct

can model multiple lifting surfaces and users can set up the optimization problem using pre-defined or user-defined objective and constraint functions.

B. Optimization Problem Formulation

To optimize aerostructural performance, we minimize the fuel burn subject to realistic constraints. Given a nominal range (in this case, 1800 km), we can compute the fuel weight needed to fly this mission using the Breguet range equation. Since this is a propeller-driven aircraft, we compute an equivalent jet thrust specific fuel consumption TSFC [24] given by

$$\text{TSFC} = C_{power}\frac{V}{\eta_p},$$

where C_{power} is the power specific fuel consumption, V is the velocity, and η_p (fixed at 0.7 here) is the propeller efficiency. Then the fuel weight W_f is computed using the Breguet range equation [24] given by

$$W_f = (W_0 + W_s)\left[\exp\left(\frac{R \cdot \text{TSFC}}{V}\left(\frac{L}{D}\right)^{-1}\right) - 1\right],$$

where W_0 is the aircraft empty weight, W_s is the structural spar weight, R is the range, L is the lift, and D is the drag. The computed W_f value is the amount of fuel burn needed to fly a conventional mission of the provided range. We select fuel burn as the objective function because it captures the tradeoffs between aerodynamic and structural performance in a realistic manner. When controlling the aerodynamic twist and structural thickness, we can decrease fuel burn by increasing $\frac{L}{D}$ or by decreasing W_s.

The inputs for the deterministic optimization problem in this work are the eight design variables $\mathbf{d} = [d_1, \ldots, d_8] \in \mathcal{D} \subseteq \mathbb{R}^8$, where $\mathcal{D}$ denotes the design space as described in Table 2. Sweep and angle of attack are scalar design variables that affect the wing design and flight conditions, respectively. Instead of directly controlling the aerodynamic and structural meshes for twist and thickness, we use a pair of b-splines to produce smooth distributions from a smaller number of control points. This allows us to choose the number of b-spline control points for the twist and thickness distributions without changing the analysis mesh sizes. In this paper, we use three b-spline control points each for both the twist and the thickness distributions.

Table 2 Bounds of the eight design variables for the ScanEagle aircraft.

Design variable	Description	Lower bound	Upper bound	Units
d_1				
d_2	structural spar thickness control points	1	10	mm
d_3				
d_4				
d_5	aerodynamic twist control points	-5	10	degrees
d_6				
d_7	angle of attack	0	10	degrees
d_8	wing sweep	10	30	degrees

To ensure that the obtained design is realistic, we require that three performance requirements are satisfied at the optimal design. Firstly, we ensure that the structural spar does not fail by comparing the computed von Mises stresses (σ_{VM}) to the allowable yield stress (σ_{yield}) in each element. We aggregate these structural failure constraints into a single constraint using a Kreisselmeier–Steinhauser (KS) function [25]. Secondly, the lift L generated must be greater than or equal to the total weight W so that the aircraft can at least sustain level flight for the cruise portion of the mission. Having the capacity to generate more lift than the total weight of the aircraft is allowable because the balance can be controlled with engine throttle settings and the angle of attack. Thirdly, we also enforce a coefficient of moment C_M constraint so that the aircraft is trimmed at the nominal flight condition. With this constraint, the nominal flying shape does not induce a pitching moment. For aircraft with tails, the tail incidence angle can vary to satisfy the C_M constraint, but due to the lack of a tail we must use a combination of wing sweep and aerodynamic twist to satisfy the constraint

here. The deterministic optimization problem formulation is given by

$$\begin{aligned} \min_{\mathbf{d}\in\mathcal{D}} \quad & f(\mathbf{d}) \\ \text{subject to} \quad & \frac{\text{KS}(\sigma_{VM}) - \sigma_{yield}}{\sigma_{yield}} \leq 0, \\ & \frac{W - L}{W} \leq 0, \\ & C_M = 0, \\ & \mathbf{d}_{lb} \leq \mathbf{d} \leq \mathbf{d}_{ub}, \end{aligned} \tag{1}$$

where f is the fuel burn for the tailless aircraft, and $\mathbf{d}_{lb}$ and $\mathbf{d}_{ub}$ represent the lower and upper bounds for the design variables, respectively. Figure 4 shows the extended design structure matrix (XDSM) [26] diagram corresponding to deterministic aerostructural optimization.

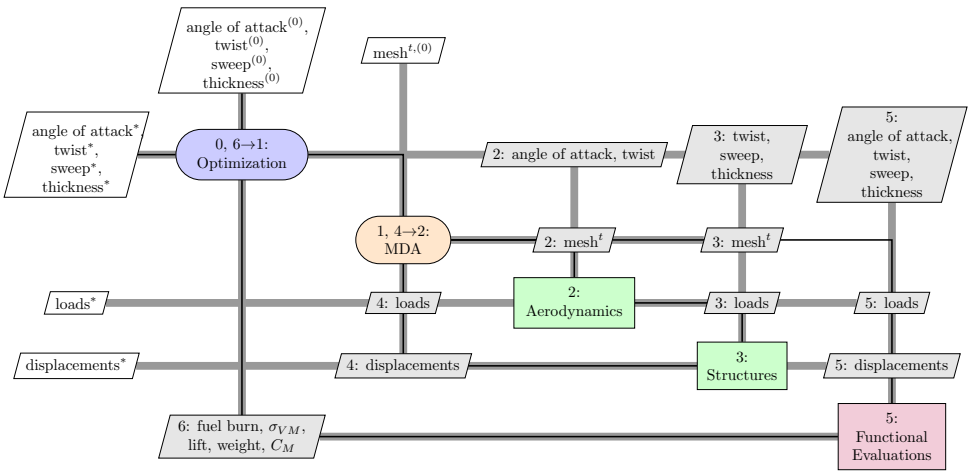

Fig. 4 XDSM diagram for deterministic aerostructural optimization. The numbers in the diagonal blocks correspond to the order of execution. The black line follows the analysis execution path whereas the thicker gray lines show data-passing paths. The default solver for the multidisciplinary analysis (MDA), shown here in the center block loop, is Gauss–Seidel. The optimal results are outputted as represented by the values with *. See [26] for more details on how to interpret this figure.

For the OUU problem formulation, the inputs for the system are the eight design variables $\mathbf{d}$ as given in Table 2 and the six uncertain input random variables $\mathbf{Z}$ as defined in Table 3. The random variables are represented by independent truncated normal distributions with lower and upper bounds defined by two standard deviations from the mean. The manufacturing uncertainty is captured by the variability in Young's modulus E, shear modulus G, material mass density ρ_{mass}, and aircraft empty weight W_0. The variation in operating conditions is captured by the uncertainty in Mach number M and thrust specific fuel consumption $TSFC$.

In this work, the robust optimization formulation considers a linear combination of the mean $\mathbb{E}[.]$, and the square root of the variance $\sqrt{\mathbb{V}\text{ar}[.]}$ (i.e., the standard deviation) of the quantity of interest as given by

$$\begin{aligned} \min_{\mathbf{d}\in\mathcal{D}} \quad & \mathbb{E}[f(\mathbf{d},\mathbf{Z})] + \eta\sqrt{\mathbb{V}\text{ar}[f(\mathbf{d},\mathbf{Z})]} \\ \text{subject to} \quad & \mathbb{E}[g_1(\mathbf{d},\mathbf{Z})] + \eta\sqrt{\mathbb{V}\text{ar}[g_1(\mathbf{d},\mathbf{Z})]} \leq 0, \\ & \mathbb{E}[g_2(\mathbf{d},\mathbf{Z})] \leq 0, \\ & \mathbb{E}[h(\mathbf{d},\mathbf{Z})] = 0, \\ & \mathbf{d}_{lb} \leq \mathbf{d} \leq \mathbf{d}_{ub}. \end{aligned} \tag{2}$$

The inequality constraint $g_1 \leq 0$ is used to avoid structural failure, and $g_2 \leq 0$ is used to satisfy the lift constraint. The equality constraint $h = 0$ ensures that the moment coefficient is equal to zero. There are several ways of formulating the

Table 3 Truncated normal distribution parameters of the uncertain random variables for the ScanEagle aircraft with lower and upper bounds defined by two standard deviations from the mean.

Random variable	Description	Mean	Standard deviation	Units
E	Young's modulus	85	5	GPa
G	shear modulus	25	1	GPa
ρ_{mass}	material mass density	1600	50	kg/m^3
W_0	aircraft operating empty weight	10	0.2	kg
M	Mach number	0.071	0.005	–
$TSFC$	thrust specific fuel consumption	0.3036	0.00607	1/hr

stochastic constraints in the optimization problem in terms of the risk of violating the performance requirements (robust or reliability constraints, penalty method to combine them into a single objective, etc). We use a robust constraint formulation for all the stochastic constraints. For the lift and moment coefficient constraints, we consider the mean value of the performance metric. For the structural failure constraint in this stochastic setup, instead of the commonly used safety factor approach, we use a robust constraint formulation to ensure that the performance requirement is satisfied up to η standard deviations from the mean.

The objective and the constraints depend on the mean and the variance, which require uncertainty propagation of the random variables through the system. In most cases, numerical approaches are used to compute estimates of these statistics for a specified mean squared error (MSE) because analytic solutions for the statistics are not available. The next section describes Monte-Carlo-simulation-based approaches for robust optimization.

III. Multifidelity Robust Optimization

Robust optimization involves solving for the required statistics for each design $\mathbf{d}_t$, where t is the current optimization iteration. The required statistics for a given design variable $\mathbf{d}_t$ are the mean, i.e., $\mathbb{E}[.]$ and the variance, i.e., $\mathbb{V}\text{ar}[.]$ estimates for f and g_1, and the mean estimates for g_2 and h. In this case, the required statistics for the constraints are estimated using the same set of samples as that for the objective because f, g_1, g_2, and h are all obtained at the same time as system outputs from a single analysis. Section III.A discusses the regular Monte Carlo simulation approach using a single high-fidelity model for estimating the statistics. Section III.B describes the multifidelity Monte Carlo method that uses information from the low-fidelity models to reduce the cost for estimating the statistics while maintaining the same MSE as the regular high-fidelity Monte Carlo approach. Implementation details for the multifidelity method are provided in Section III.C.

A. High-Fidelity Monte Carlo Simulation Approach

Given m independent and identically distributed (i.i.d.) high-fidelity samples $f(\mathbf{d}_t, \mathbf{z}_j)$ for $j = 1, \ldots, m$, Monte Carlo simulation can be used to obtain estimates for the mean and variance of f at $\mathbf{d}_t$. The Monte Carlo estimator of the mean of f is given by

$$\hat{s}_m(\mathbf{d}_t) = \frac{1}{m}\sum_{j=1}^{m} f(\mathbf{d}_t, \mathbf{z}_j). \tag{3}$$

The subscript m in the estimator denotes that m samples were used to compute it. Note that the Monte Carlo estimator is an unbiased estimator for the mean, which means that the expected value of the estimator's error is zero, i.e., $\mathbb{E}[\hat{s}_m(\mathbf{d}_t)] = \mathbb{E}[f(\mathbf{d}_t, \mathbf{Z})]$. We measure the error in the mean estimator using the MSE, which in this case is equal to the variance of the mean estimator because of its unbiased nature. That is,

$$J_1 = \text{MSE}[\hat{s}_m(\mathbf{d}_t)] = \mathbb{V}\text{ar}[\hat{s}_m(\mathbf{d}_t)] = \frac{\sigma^2}{m}, \tag{4}$$

where σ^2 is the variance of $f(\mathbf{d}_t, \mathbf{Z})$. Equation (4) shows that the accuracy of the estimator depends on the variance of f (which we cannot control) and on the number of Monte Carlo samples (which we choose). It also shows that many samples will be needed to achieve a low error, which is why uncertainty quantification is expensive.

The estimate of the unbiased sample variance of f, which is also needed in our robust optimization objective function, is given by

$$\hat{v}_m(\mathbf{d}_t) = \frac{1}{m-1}\sum_{j=1}^{m}\left(f(\mathbf{d}_t,\mathbf{z}_j) - \hat{s}_m(\mathbf{d}_t)\right)^2, \tag{5}$$

where the subscript m in the estimator denotes that m samples were used to compute it. In order to define the Monte Carlo estimator for the variance of f, we introduce an auxiliary variable given by

$$b_m(\mathbf{d}_t,\mathbf{z}_j) = \frac{m}{m-1}\left(f(\mathbf{d}_t,\mathbf{z}_j) - \hat{s}_m(\mathbf{d}_t)\right)^2. \tag{6}$$

Now, the estimator of the variance given by Equation (5) can be redefined as

$$\hat{v}_m(\mathbf{d}_t) = \frac{1}{m}\sum_{j=1}^{m} b_m(\mathbf{d}_t,\mathbf{z}_j). \tag{7}$$

Similar to the mean estimate, the Monte Carlo estimate of the variance is also unbiased, which means that the expected error in our variance estimate is zero (i.e., $\mathbb{E}[\hat{v}_m(\mathbf{d}_t)] = \mathbb{V}\text{ar}[f(\mathbf{d}_t,\mathbf{Z})]$). We measure the accuracy of the variance estimator through its MSE. Again, because of the unbiased nature of the variance estimator, its MSE is given by the variance of $\hat{v}_m(\mathbf{d}_t)$. Assuming that different sets of $\mathbf{Z}$ realizations are used for $\hat{s}_m(\mathbf{d}_t)$ and $\hat{v}_m(\mathbf{d}_t)$ (or, equivalently, that the $b_m(\mathbf{d}_t,\mathbf{Z})$ samples are i.i.d.), the MSE can be defined similarly to that of $\hat{s}_m(\mathbf{d}_t)$ as given by

$$J_2 = \text{MSE}[\hat{v}_m(\mathbf{d}_t)] = \mathbb{V}\text{ar}[\hat{v}_m(\mathbf{d}_t)] = \frac{\tau^2}{m}, \tag{8}$$

where τ^2 is the variance of the auxiliary variable $b_m(\mathbf{d}_t,\mathbf{Z})$. Note that in this work, the same set of realizations of random samples of $\mathbf{Z}$ are used for $\hat{s}_m(\mathbf{d}_t)$ and $\hat{v}_m(\mathbf{d}_t)$, making the $b_m(\mathbf{d}_t,\mathbf{Z})$ samples not i.i.d. MSE$[\hat{v}_m(\mathbf{d}_t)]$ can be defined as the variance of sample variance in terms of the second and fourth moments taking into account that the $b_m(\mathbf{d}_t,\mathbf{Z})$ samples are not i.i.d. [27]. However, as we mention in Section III.C, we need at least crude initial sample estimates for the variances in order to implement this method and it is very difficult to get even a crude estimate of fourth moments with a small set of samples. Hence, we use the definition of MSE given by Equation (8) neglecting that our samples are not i.i.d.

We define a total error metric for estimating both the mean and the variance as the sum of the MSE of the mean and the variance estimates. The error metric J_m is given by

$$J_m = J_1 + J_2 = \text{MSE}[\hat{s}_m(\mathbf{d}_t)] + \text{MSE}[\hat{v}_m(\mathbf{d}_t)] = \frac{\sigma^2+\tau^2}{m}, \tag{9}$$

where the subscript m denotes that we use m samples to compute the estimators (and again we note that we use the same set of samples to compute both mean and variance). The chosen form of the error metric J_m in Equation (9) is motivated by the form of the OUU objective function in Equation (2) (noting that we cannot compute the MSE of the OUU objective function directly). In our implementation, we specify the tolerance on J_m and compute the required number of samples. In order to ensure that the error in the estimate is below a specified tolerance J_{tol}, the required number of Monte Carlo samples is

$$m^* = \frac{\sigma^2+\tau^2}{J_{tol}}. \tag{10}$$

B. Multifidelity Monte Carlo Approach

This section develops a multifidelity Monte Carlo (MFMC) method for more efficient estimates of the required statistics in robust optimization while maintaining the same level of accuracy (fixed MSE). The proposed method is an extension of the MFMC method [3, 14] to estimate both the mean and the variance using the same set of samples when multiple fidelities are available.

Consider k models $f^{(1)},\ldots,f^{(k)}$ with $f^{(1)}$ being the highest fidelity and no known hierarchy for the other $k-1$ models. For a given design $\mathbf{d}_t$, we order the models such that

$$|\rho_{1,1}| + |q_{1,1}| > \cdots > |\rho_{1,k}| + |q_{1,k}|, \tag{11}$$

where $\rho_{1,i}$ is the correlation coefficient between the highest fidelity $f^{(1)}(\mathbf{d}_t, \mathbf{Z})$ and i^{th} fidelity $f^{(i)}(\mathbf{d}_t, \mathbf{Z})$, and $q_{1,i}$ is the auxiliary variables correlation coefficient between the highest fidelity $b_m^{(1)}(\mathbf{d}_t, \mathbf{Z})$ and i^{th} fidelity $b_m^{(i)}(\mathbf{d}_t, \mathbf{Z})$. This means that as the index in the ordering of the models increases, their correlation with the high-fidelity model decreases. In this case, the correlation with the high-fidelity model defines our level of confidence in that particular model.

Once the ordering is established for design $\mathbf{d}_t$, we can see that it makes sense to use a lower fidelity model if and only if it is cheaper to evaluate than the higher fidelities. Let the cost incurred for evaluating model $f^{(i)}$ be $w_i \in \mathbb{R}_+$. After reordering the models according to Equation (11), the costs should satisfy $w_1 \geq \cdots \geq w_k \geq 0$ to make sure that a lower fidelity model is cheaper to evaluate. Otherwise, models with higher cost and lower correlation are removed from the set of available fidelities for design $\mathbf{d}_t$.

Define $\mathbf{m} = [m_1, \ldots, m_k]^T \in \mathbb{N}^k$ as the vector of sample sizes for different fidelities such that $0 < m_1 \leq \cdots \leq m_k$. Let $\mathbf{z}_1, \ldots, \mathbf{z}_{m_k}$ be m_k realizations of the random variable $\mathbf{Z}$. Then each model $f^{(i)}$ is evaluated at the first m_i samples to obtain the corresponding system outputs. Thus, the highest fidelity is evaluated least number of times and the rest of the fidelities are evaluated with increasing frequency as their index in the ordering increases. Then the outputs from the different fidelities are used to define the Monte Carlo estimators,

$$\hat{s}_{m_i}^{(i)}(\mathbf{d}_t) = \frac{1}{m_i} \sum_{j=1}^{m_i} f^{(i)}(\mathbf{d}_t, \mathbf{z}_j), \tag{12}$$

$$\hat{v}_{m_i}^{(i)}(\mathbf{d}_t) = \frac{1}{m_i} \sum_{j=1}^{m_i} b_{m_i}^{(i)}(\mathbf{d}_t, \mathbf{z}_j), \tag{13}$$

where $\hat{s}_{m_i}^{(i)}(\mathbf{d}_t)$ denotes the mean estimate of $f^{(i)}$ computed with m_i samples and $\hat{v}_{m_i}^{(i)}(\mathbf{d}_t)$ denotes the variance estimate of $f^{(i)}$ computed with m_i samples. Following similar notation, the auxiliary variable $b_{m_i}^{(i)}(\mathbf{d}_t, \mathbf{z}_j) = \frac{m_i}{m_i - 1} \left(f^{(i)}(\mathbf{d}_t, \mathbf{z}_j) - \hat{s}_{m_i}^{(i)}(\mathbf{d}_t) \right)^2$ for each fidelity $i = 1, \ldots, k$.

The Monte Carlo estimators from the different fidelities are combined using the control variates method to reduce the estimator variance. The MFMC estimate for the mean is given by

$$\hat{s}_{MF}(\mathbf{d}_t) = \hat{s}_{m_1}^{(1)}(\mathbf{d}_t) + \sum_{i=2}^{k} \alpha_i \left(\hat{s}_{m_i}^{(i)}(\mathbf{d}_t) - \hat{s}_{m_{i-1}}^{(i)}(\mathbf{d}_t) \right), \tag{14}$$

where $\alpha_2, \ldots, \alpha_k$ are the control variate coefficients for the different fidelities for the mean estimate. The MFMC estimate for the variance is given by

$$\hat{v}_{MF}(\mathbf{d}_t) = \hat{v}_{m_1}^{(1)}(\mathbf{d}_t) + \sum_{i=2}^{k} \beta_i \left(\hat{v}_{m_i}^{(i)}(\mathbf{d}_t) - \hat{v}_{m_{i-1}}^{(i)}(\mathbf{d}_t) \right), \tag{15}$$

where $\beta_2, \ldots, \beta_k$ are the control variate coefficients for the different fidelities for the variance estimate. Figure 5 shows the MFMC method for estimating the mean for a given design variable $\mathbf{d}_t$. The MFMC estimate for the variance follows a similar flow.

Now, we need to choose values for the samples sizes for each fidelity $(m_1, \ldots, m_k)$ and control variate coeficients $(\alpha_2, \ldots, \alpha_k, \beta_2, \ldots, \beta_k)$ in order to implement the MFMC estimates. This is done by minimizing the error in the MFMC mean and variance estimators while taking into account the correlations with high-fidelity model and the costs of the different models. Similar to the Monte Carlo error metric in Equation (9), the MFMC error metric can be defined as

$$J(\mathbf{m}, \alpha_2, \ldots, \alpha_k, \beta_2, \ldots, \beta_k) = \text{MSE}[\hat{s}_{MF}(\mathbf{d}_t)] + \text{MSE}[\hat{v}_{MF}(\mathbf{d}_t)] = \mathbb{V}\text{ar}[\hat{s}_{MF}(\mathbf{d}_t)] + \mathbb{V}\text{ar}[\hat{v}_{MF}(\mathbf{d}_t)]. \tag{16}$$

The derivation for the variance of the MFMC estimate of the mean ($\mathbb{V}\text{ar}[\hat{s}_{MF}(\mathbf{d}_t)]$) is available in [14]. The variance of the MFMC estimate of the variance ($\mathbb{V}\text{ar}[\hat{v}_{MF}(\mathbf{d}_t)]$) can be similarly derived neglecting that our $b_{m_i}^{(i)}(\mathbf{d}_t, \mathbf{Z})$ samples are not i.i.d. [28]. We do not repeat those derivations here, but just give the resulting sample sizes and control variate coefficients as follows.

The optimal sample sizes $\mathbf{m}^*$ and the optimal coefficients, α_i^* and β_i^* for $i = 2, \ldots, k$ that minimize the error metric

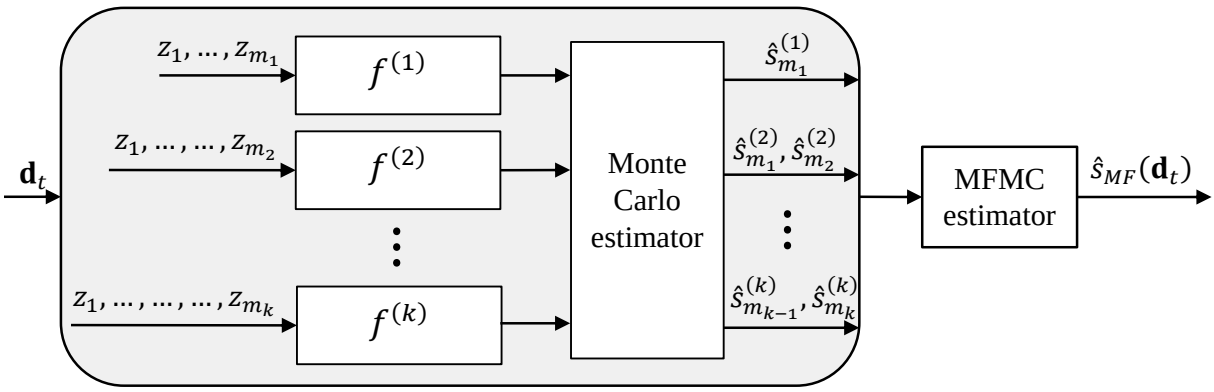

Fig. 5 MFMC method for estimating the mean for given design variable $\mathbf{d}_t$.

given in Equation (16) for a given budget p can be found (using Karush-Kuhn-Tucker conditions) to be

$$\alpha_i^* = \frac{\rho_{1,i}\sigma_1}{\sigma_i} \tag{17}$$

$$\beta_i^* = \frac{q_{1,i}\tau_1}{\tau_i} \tag{18}$$

$$r_i^* = \frac{m_i^*}{m_1^*} = \sqrt{\frac{w_1(\sigma_1^2(\rho_{1,i}^2 - \rho_{1,i+1}^2) + \tau_1^2(q_{1,i}^2 - q_{1,i+1}^2))}{w_i(\sigma_1^2(1-\rho_{1,2}^2) + \tau_1^2(1-q_{1,2}^2))}} \tag{19}$$

$$m_1^* = \frac{p}{\mathbf{w}^T\mathbf{r}^*} \tag{20}$$

$$m_i^* = m_1^* r_i^*. \tag{21}$$

For evaluating these optimal allocation and optimal coefficients, set $\rho_{1,k+1} = 0$ and $q_{1,k+1} = 0$. The MFMC method will allocate most samples to the low-fidelity model that best balances low cost and high correlation.

Given a value of tolerance in the error J_{tol} the value of required budget p_{req} can be found by substituting the optimal solution into Equation (16) and solving to get

$$p_{req} = \frac{\mathbf{w}^T\mathbf{r}^*\left[\sigma_1^2 + \tau_1^2 + \sum_{i=2}^{k}\left(\frac{1}{r_i^*} - \frac{1}{r_{i-1}^*}\right)\left(\rho_{1,i}^2\sigma_1^2 + q_{1,i}^2\tau_1^2\right)\right]}{J_{tol}} \tag{22}$$

This required budget is to ensure that the error in the estimators is below J_{tol}.

C. Implementation Details

In order to implement the MFMC method for a given design $\mathbf{d}_t$, we need the values for σ_i, τ_i, $\rho_{1,i}$, and $q_{1,i}$ for all the fidelities $i = 1, \ldots, k$, which are usually not known analytically. We use an inital set of m_{init} random realizations of $\mathbf{Z}$ to get sample estimates of these quantities. Apart from these quantities, we also need the costs w_i associated with each fidelity, which can be found by timing these initial runs. As shown in [14], these crude sample estimates are sufficient to get the values of optimal allocation and the optimal coefficients, and small perturbations in these sample estimates typically have small effects on the MFMC allocations. Then the MFMC method is applied to get the mean and variance estimates that are used to compute the robust optimization objective function and constraints for the given design $\mathbf{d}_t$ as summarized in Algorithm 1.

IV. Numerical Results

We demonstrate the multifidelity robust optimization method on the ScanEagle tailless aircraft application and compare the performance of the proposed method with the regular Monte Carlo estimator method. We consider three different fidelities for the ScanEagle analysis by varying the wing mesh defined by the number of evenly-spaced spanwise

Algorithm 1 MFMC approach for estimating the mean and the variance

procedure MeanVarMFMC($f^{(1)}, \ldots, f^{(k)}, \mathbf{d}_t, J_{tol}, \sigma_1, \ldots, \sigma_k, \tau_i, \ldots, \tau_k, \rho_{1,i}, \ldots, \rho_{1,k}, q_{1,i}, \ldots, q_{1,k}$)
  Ensure that the models $f^{(1)}, \ldots, f^{(k)}$ are ordered according to Equation (11)
  Set $\rho_{1,k+1} = 0$ and $q_{1,k+1} = 0$
  Compute optimal coefficients α_i^* and β_i^* using Equations (17)- (18)
  Compute optimal values for ratios of sample sizes r_i for $i = 1, \ldots, k$ using Equation (19)
  Compute required budget p_{req} to ensure that the error metric meets the specified tolerance J_{tol} using Equation (22)
  Compute optimal sample sizes $\mathbf{m}^*$ using Equations (20)- (21) and p_{req}
  Round up $\mathbf{m}^*$ to the nearest integer greater than or equal to it.
  Sample $\mathbf{z}_1, \ldots, \mathbf{z}_{m_k}$ realizations of $\mathbf{Z}$
  Evaluate model $f^{(i)}$ at the first $\mathbf{z}_1, \ldots, \mathbf{z}_{m_i}$ samples for $i = 1, \ldots, k$
  Compute MFMC estimate for mean $\hat{s}_{MF}(\mathbf{d}_t)$ using Equation (14) and variance $\hat{v}_{MF}(\mathbf{d}_t)$ using Equation (15)
  return $\hat{s}_{MF}(\mathbf{d}_t), \hat{v}_{MF}(\mathbf{d}_t)$
end procedure

and chordwise points. Details for the different models and the average cost associated with each fidelity are summarized in Table 4. The high-fidelity model $f^{(1)}$ is around 35 times more expensive than the low-fidelity model $f^{(2)}$ and around 77 times more expensive than the low-fidelity model $f^{(3)}$. These simulations were run on a desktop machine with an Intel i7-4790K 4-core 4.0 GHz CPU and 32 GB of RAM.

Table 4 Different fidelity models and their cost for ScanEagle analysis.

Model	Number of spanwise points	Number of chordwise points	Evaluation cost (s)
High-fidelity model $f^{(1)}$	61	7	4.74×10^{-1}
Low-fidelity model $f^{(2)}$	21	3	1.33×10^{-2}
Low-fidelity model $f^{(3)}$	5	2	6.15×10^{-3}

The outer-loop stochastic optimization problem given by Equation (2) is solved through sequential local searches using the basin-hopping [29] algorithm with seven restarts. The derivative-free constrained optimization by linear approximation (COBYLA) [30] algorithm with maximum iterations set to 50 is used for the local searches. These algorithms are implemented from the *scipy.optimize* toolbox in Python. The Monte Carlo method (Section III.A) and MFMC method (Section III.B) are used for the inner-loop uncertainty propagation to estimate the mean and the variance. The tolerance on the error is set at $J_{tol} = 10^{-4}$ for both the Monte Carlo and the MFMC methods in order to maintain the same level of accuracy. For the MFMC method, an initial set of 20 samples are used to sample estimates indicated in Section III.C. Two formulations of the robust optimization problem given in Equation (2) are solved: (1) with $\eta = 2$, and (2) with $\eta = 3$.

The convergence of the robust fuel burn objective function as a function of the computational effort is shown in Figure 6, where the computational effort is represented by equivalent number of high-fidelity solves. It can be seen that in both cases the multifidelity robust optimization method locates the best design with around 90% computational savings as compared to the regular Monte Carlo estimator method. For the $\eta = 2$ case, the regular Monte Carlo method takes more than 8 hours to locate the best design as compared to around 47 minutes using the multifidelity method on our machine. For the $\eta = 3$ case, the regular Monte Carlo method takes 2.9 hours to locate the best design as compared to around 23 minutes using the multifidelity method on our machine.

The computational effort is examined in more detail by plotting it for each optimization iteration in Figure 7. It can be clearly seen that the computational effort for the Monte Carlo estimator is always more than that of the MFMC estimator in this case. The reason for the low computational effort for the MFMC method is due to the use of cheaper low-fidelity models to speed-up the estimators. The allocation of resources between the different fidelities quantified by the number of samples for each is shown in Figure 8. It can be seen that the cheapest model $f^{(3)}$ is evaluated most (hundreds of times per iteration), followed by the model $f^{(2)}$, and the expensive high-fidelity model $f^{(1)}$ is evaluated very few times. Note that we used at least 20 initial samples for each fidelity in the MFMC method to calculate the parameters noted in Section III.C. The number of samples required for some of the models could be less than 20, if the

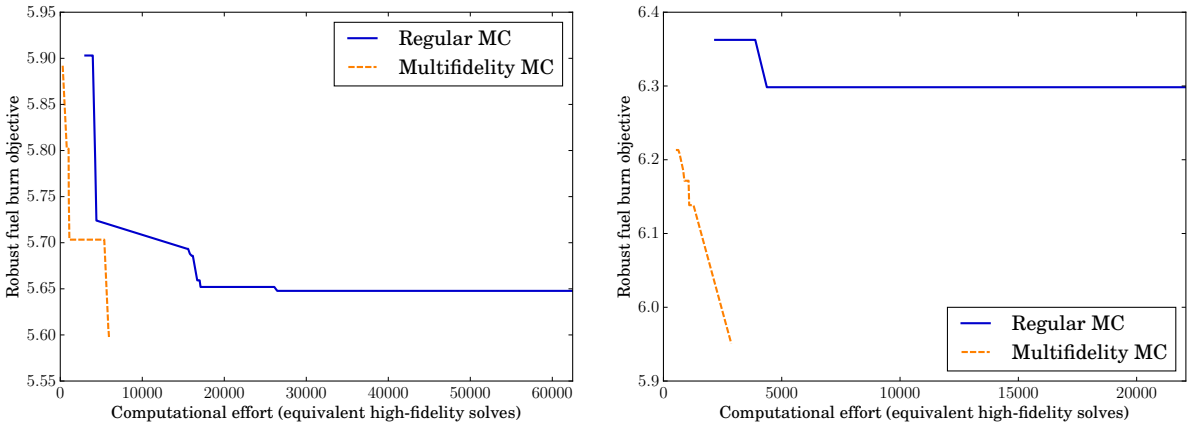

(a) $\eta = 2$ (b) $\eta = 3$

Fig. 6 Comparison of convergence histories of robust optimization using the regular Monte Carlo (regular MC) estimator and the multifidelity estimator.

cheaper models are highly correlated to the high-fidelity model. However, since at least 20 samples are used here for every model (more than required for some models for certain designs given the J_{tol}), this can lead to a lower error in the MFMC estimates than the specified J_{tol}.

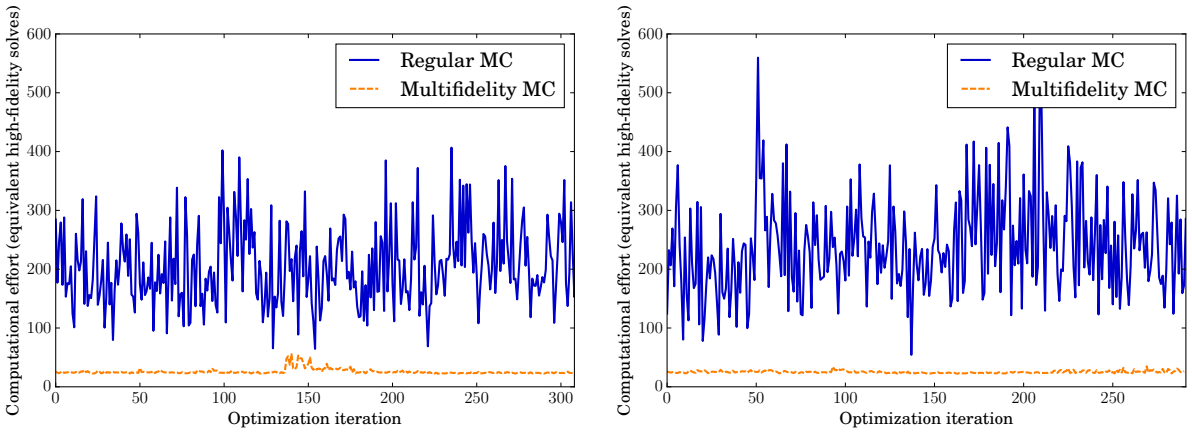

(a) $\eta = 2$ (b) $\eta = 3$

Fig. 7 Comparison of computational effort required in each optimization iteration.

Figures 9 and 10 show the details of the robust objective and constraint values associated with each design visited during the optimization process. Note that as seen before, the computational efforts for the multifidelity method is substantially less than that of the regular Monte Carlo method in these plots. Table 5 shows the best design configurations for the ScanEagle aircraft obtained through the different robust optimization methods along with the initial design. Using the multifidelity robust optimization method, the expected fuel burn decreases from 6.09 kg for the initial design to 5.32 kg for the best design obtained from the $\eta = 2$ case, and to 5.53 kg for the best design obtained from the $\eta = 3$ case. For all the cases, the constraints are satisfied, i.e., the expected value of the moment coefficient constraint for the best design is approximately zero, the expected value of the lift constraint is below zero and the structural failure constraint is satisfied up to η standard deviations of the mean. The initial design in this case does not satisfy the moment constraint. Note that there are differences between the best designs obtained using the Monte Carlo method compared to

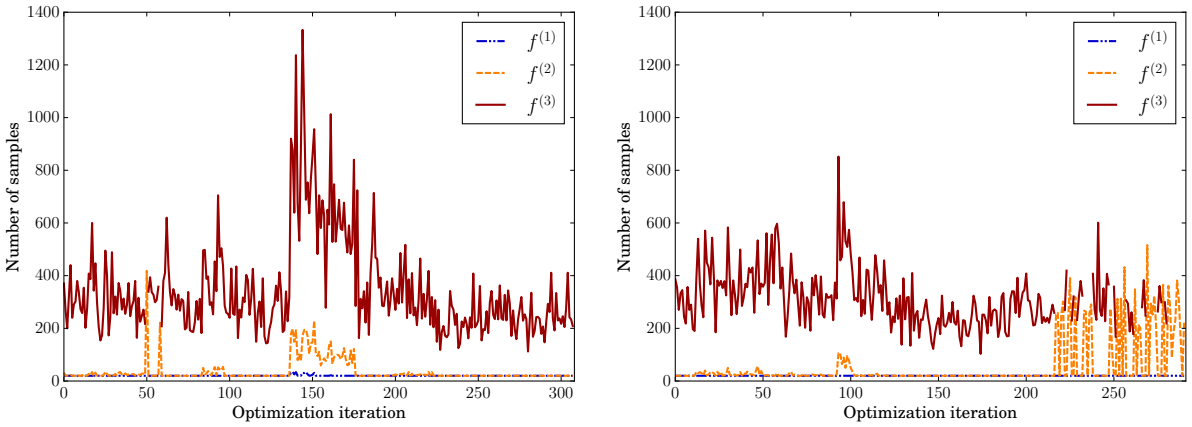

(a) $\eta = 2$ (b) $\eta = 3$

Fig. 8 Number of samples required for each fidelity per optimization iteration for the multifidelity robust optimization method.

the multifidelity method for the same value of η. This is because the best designs obtained here could be local optima of the stochastic global optimization problem, or they could correspond to unconverged solutions. Given the global nature of the design problem and the stochastic nature of the objective function, we cannot make rigorous statements about the convergence of our runs. However, the results show that the optimizer is able to achieve significant improvements in the designs, reducing both mean and variance from the initial design point. The results for the Monte Carlo method and the multifidelity method could potentially improve if we run the optimizer for longer. However, Figure 6 shows that the convergence for the regular Monte Carlo method has stalled. Continuing to run it is expensive in terms of function evaluations but not yielding improvements in the best design found. For this problem, the multifidelity approach has managed to find better designs at greatly reduced computational cost.

Figure 11 visually compares the two best design configurations obtained using the multifidelity method for the $\eta = 2$ and $\eta = 3$ cases. The spar thickness is greater for the $\eta = 3$ due to the requirement to handle higher loadings for the more extreme flight conditions. The sweep values are close to the same, which is expected to satisfy the $C_M = 0$ constraint. The increase in twist for the $\eta = 3$ is offset by a corresponding decrease in angle of attack, though the twist distribution does vary more smoothly in this case. For the $\eta = 3$ case, the effective twist at the wingtips is lessened and acts to unload the outboard wing, allowing the optimizer to handle higher loading conditions without failing structurally.

V. Conclusions

This paper presented a multifidelity robust optimization method for a ScanEagle tailless aircraft application in the presence of uncertainties in manufacturing and operating conditions. The best designs obtained using the multifidelity method decreased the expected fuel burn to 5.32 kg for the $\eta = 2$ case and 5.53 kg for the $\eta = 3$ case as compared to 6.09 kg for the initial design. The multifidelity method uses the control-variates-based MFMC to combine information from different fidelities in order to reduce the variance in the estimators used in the OUU problem objective function and constraints. The MFMC method used in this work optimally allocates resources between the different fidelities for minimizing the error in the estimates of the mean and the variance when the same set of samples is used for both. This optimal allocation depends on the costs of the low-fidelity models and their correlation to the high-fidelity model. The MFMC estimates are unbiased and substantially reduce the computational cost by sampling the cheaper low-fidelity models more. For the ScanEagle analysis, the lower fidelity models were created by using coarser discretizations of the wing mesh. In general the multifidelity method can be used with any kind of low-fidelity model. The multifidelity robust optimization method maintains the same level of accuracy as the regular Monte Carlo method but offers around 90% computational savings for the ScanEagle problem.

In this work, the multifidelity method ensures that the estimates for the statistics of the objective function are below a given tolerance on the error. However, in general we can choose the optimal allocation of resources based on whether

Table 5 Comparison of best designs obtained from different methods and the initial design used for ScanEagle.

Design variable/ Output statistic	Initial design	Monte Carlo		Multifidelity	
		$\eta = 2$	$\eta = 3$	$\eta = 2$	$\eta = 3$
d_1	5.5	1.15	6.91	1	1
d_2	5.5	3.89	5.61	1.04	1.12
d_3	5.5	3.47	5.21	3.41	4.60
d_4	2.5	-3.27	2.46	-1.59	0.55
d_5	2.5	4.62	4.58	0.34	6.37
d_6	2.5	5.64	4.99	4.50	6.30
d_7	5	3.56	4.12	5.54	2.52
d_8	20	19.13	18.54	18.73	18.35
$\mathbb{E}[f]$	6.09	5.39	5.92	5.32	5.53
$\mathbb{V}\text{ar}[f]$	2.2×10^{-2}	1.7×10^{-2}	1.6×10^{-2}	2×10^{-2}	2×10^{-2}
$\mathbb{E}[g_1]$	-0.58	-0.61	-0.56	-0.59	-0.61
$\mathbb{V}\text{ar}[g_1]$	1.5×10^{-3}	1.5×10^{-3}	1.6×10^{-3}	1.9×10^{-3}	8.3×10^{-4}
$\mathbb{E}[g_2]$	-0.23	-0.25	-0.31	-0.31	-0.31
$\mathbb{E}[h]$	-9.2×10^{-2}	-8.9×10^{-4}	-6.3×10^{-4}	-2.8×10^{-4}	-5.9×10^{-4}

the objective function or the constraints require more budget to meet their specified tolerances. This strategy will be explored in our future work.

Acknowledgement

This work has been supported in part by the Air Force Office of Scientific Research (AFOSR) MURI on managing multiple information sources of multi-physics systems, Program Manager Jean-Luc Cambier, Award Number FA9550-15-1-0038. The second author is grateful for support from the National Science Foundation Graduate Research Fellowship under Grant No. DGE-1256260.

References

[1] Alexandrov, N. M., Lewis, R. M., Gumbert, C. R., Green, L. L., and Newman, P. A., "Approximation and model management in aerodynamic optimization with variable-fidelity models," *Journal of Aircraft*, Vol. 38, No. 6, 2001, pp. 1093–1101.

[2] Queipo, N. V., Haftka, R. T., Shyy, W., Goel, T., Vaidyanathan, R., and Tucker, P. K., "Surrogate-based analysis and optimization," *Progress in Aerospace Sciences*, Vol. 41, No. 1, 2005, pp. 1–28.

[3] Ng, L. W., and Willcox, K. E., "Multifidelity approaches for optimization under uncertainty," *International Journal for Numerical Methods in Engineering*, Vol. 100, No. 10, 2014, pp. 746–772.

[4] Peherstorfer, B., Willcox, K., and Gunzburger, M., "Survey of multifidelity methods in uncertainty propagation, inference, and optimization," *SIAM Review*, 2017. (to appear).

[5] Jones, D. R., "A taxonomy of global optimization methods based on response surfaces," *Journal of Global Optimization*, Vol. 21, No. 4, 2001, pp. 345–383.

[6] Forrester, A. I., and Keane, A. J., "Recent advances in surrogate-based optimization," *Progress in Aerospace Sciences*, Vol. 45, No. 1, 2009, pp. 50–79.

[7] Lam, R., Allaire, D., and Willcox, K., "Multifidelity optimization using statistical surrogate modeling for non-hierarchical information sources," *56th AIAA/ASCE/AHS/ASC Structures, Structural Dynamics, and Materials Conference*, 2015.

[8] Poloczek, M., Wang, J., and Frazier, P., "Multi-information source optimization," *Advances in Neural Information Processing Systems*, 2017, pp. 4289–4299.

[9] Kennedy, M. C., and O'Hagan, A., "Predicting the output from a complex computer code when fast approximations are available," *Biometrika*, Vol. 87, No. 1, 2000, pp. 1–13.

[10] Eldred, M. S., "Recent advances in non-intrusive polynomial chaos and stochastic collocation methods for uncertainty analysis and design," *50th AIAA/ASME/ASCE/AHS/ASC Structures, Structural Dynamics, and Materials Conference*, 2009.

[11] Law, A. M., and Kelton, W. D., *Simulation Modeling and Analysis*, 2nd ed., McGraw-Hill New York, 1991.

[12] Giles, M. B., "Multilevel monte carlo path simulation," *Operations Research*, Vol. 56, No. 3, 2008, pp. 607–617.

[13] Tracey, B., Wolpert, D., and Alonso, J. J., "Using supervised learning to improve monte carlo integral estimation," *AIAA Journal*, Vol. 51, No. 8, 2013, pp. 2015–2023.

[14] Peherstorfer, B., Willcox, K., and Gunzburger, M., "Optimal model management for multifidelity Monte Carlo estimation," *SIAM Journal on Scientific Computing*, Vol. 38, No. 5, 2016, pp. A3163–A3194.

[15] Qian, E., Peherstorfer, B., O'Malley, D., Vesselinov, V., and Willcox, K., "Multifidelity Monte Carlo estimation of variance and sensitivity indices," Tech. Rep. TR-2017-2, ACDL, Massachusetts Institute of Technology, Cambridge, Massachusetts, 2017.

[16] Liebeck, R. H., "Design of the blended wing body subsonic transport," *Journal of Aircraft*, Vol. 41, No. 1, 2004, pp. 10–25.

[17] Boeing, "ScanEagle Unmanned Aircraft Systems," `http://www.boeing.com/farnborough2014/pdf/BDS/ScanEagle%20Backgrounder%200114.pdf`, 2013.

[18] Sobieszczanski-Sobieski, J., and Haftka, R. T., "Multidisciplinary aerospace design optimization: Survey of recent developments," *Structural Optimization*, Vol. 14, No. 1, 1997, pp. 1–23.

[19] Kenway, G. K., and Martins, J. R., "Multipoint high-fidelity aerostructural optimization of a transport aircraft configuration," *Journal of Aircraft*, 2014.

[20] Leifsson, L., Ko, A., Mason, W. H., Schetz, J. A., Grossman, B., and Haftka, R., "Multidisciplinary design optimization of blended-wing-body transport aircraft with distributed propulsion," *Aerospace Science and Technology*, Vol. 25, No. 1, 2013, pp. 16–28.

[21] Martins, J. R., and Lambe, A. B., "Multidisciplinary design optimization: A survey of architectures," *AIAA Journal*, , No. 9, 2013, pp. 2049–2075.

[22] Jasa, J. P., Hwang, J. T., and Martins, J. R. R. A., "Open-source coupled aerostructural optimization using Python," *Structural and Multidisciplinary Optimization*, 2018. (Submitted).

[23] Heath, C. M., and Gray, J. S., "OpenMDAO: Framework for Flexible Multidisciplinary Design, Analysis and Optimization Methods," *8th AIAA Multidisciplinary Design Optimization Specialist Conference (MDO)*, Honolulu, Hawaii, 2012, pp. 1–13.

[24] Raymer, D. P., *Aircraft Design: A Conceptual Approach*, 3rd ed., AIAA, Inc., Reston, VA, 1999.

[25] Kreisselmeier, G., and Steinhauser, R., "Systematic control design by optimizing a vector performance index," *Computer Aided Design of Control Systems*, Elsevier, 1980, pp. 113–117.

[26] Lambe, A. B., and Martins, J. R., "Extensions to the design structure matrix for the description of multidisciplinary design, analysis, and optimization processes," *Structural and Multidisciplinary Optimization*, Vol. 46, No. 2, 2012, pp. 273–284.

[27] Mood, A., Graybill, F., and Boes, D., *Introduction to the Theory of Statistics*, 3rd ed., McGraw-Hill, Inc., 1974.

[28] Chaudhuri, A., and Willcox, K., "Multifidelity robust optimization," 2018. (In preparation).

[29] Wales, D. J., and Doye, J. P., "Global optimization by basin-hopping and the lowest energy structures of Lennard-Jones clusters containing up to 110 atoms," *The Journal of Physical Chemistry A*, Vol. 101, No. 28, 1997, pp. 5111–5116.

[30] Powell, M. J., "A direct search optimization method that models the objective and constraint functions by linear interpolation," *Advances in Optimization and Numerical Analysis*, Springer, 1994, pp. 51–67.

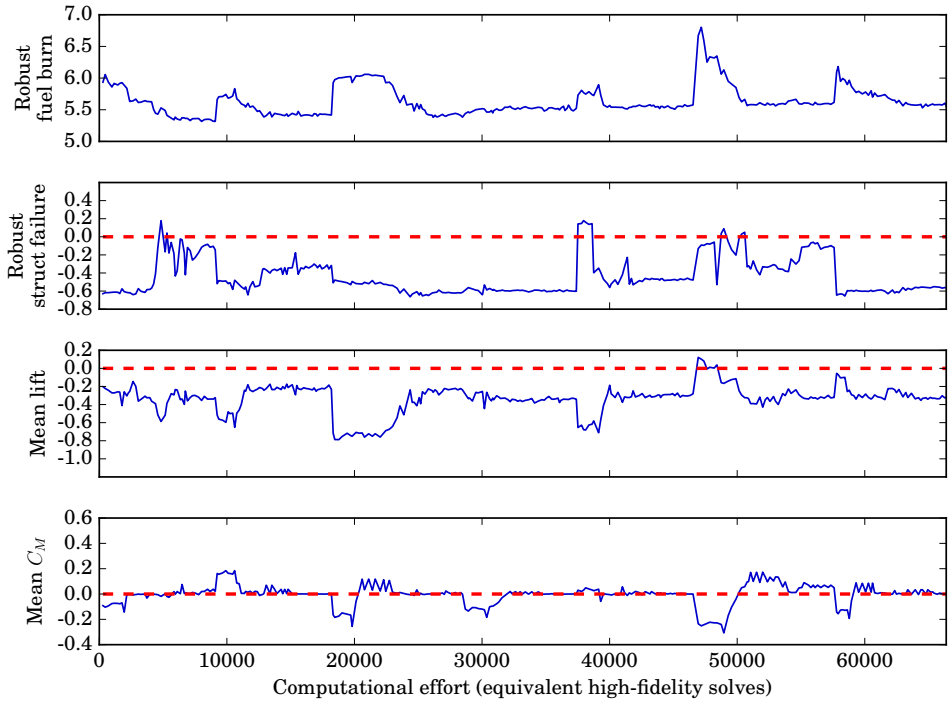

(a) Regular Monte Carlo

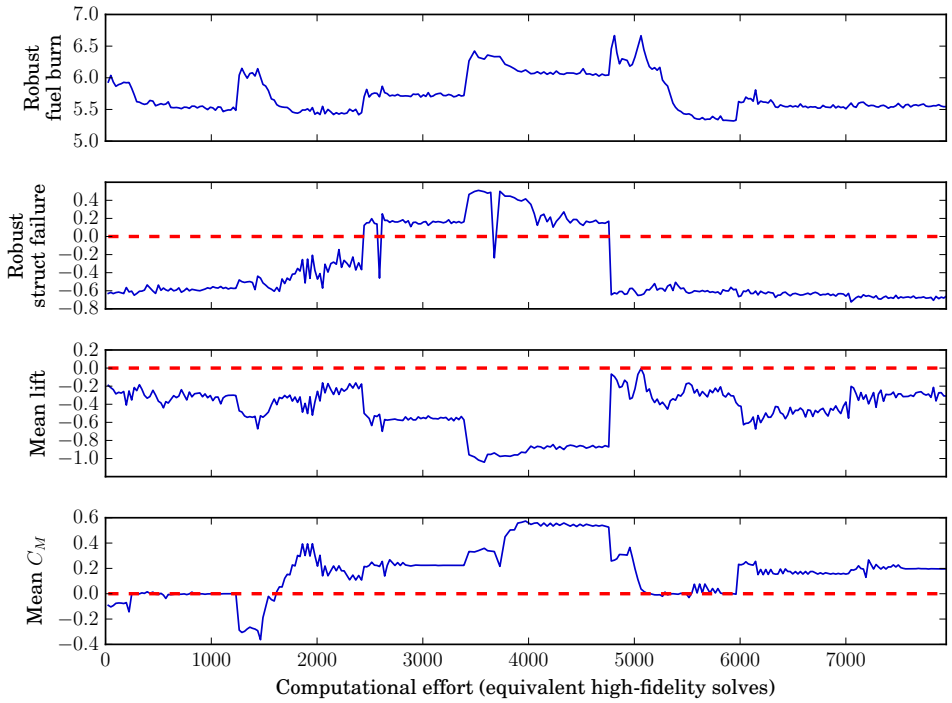

(b) Multifidelity

Fig. 9 Optimization history of the robust objective function and constraints for $\eta = 2$ associated with each visited design versus computational effort. Red dashed line shows the feasibility limit for the constraints. Note that the computational effort on the x-axis of the two plots have different magnitudes.

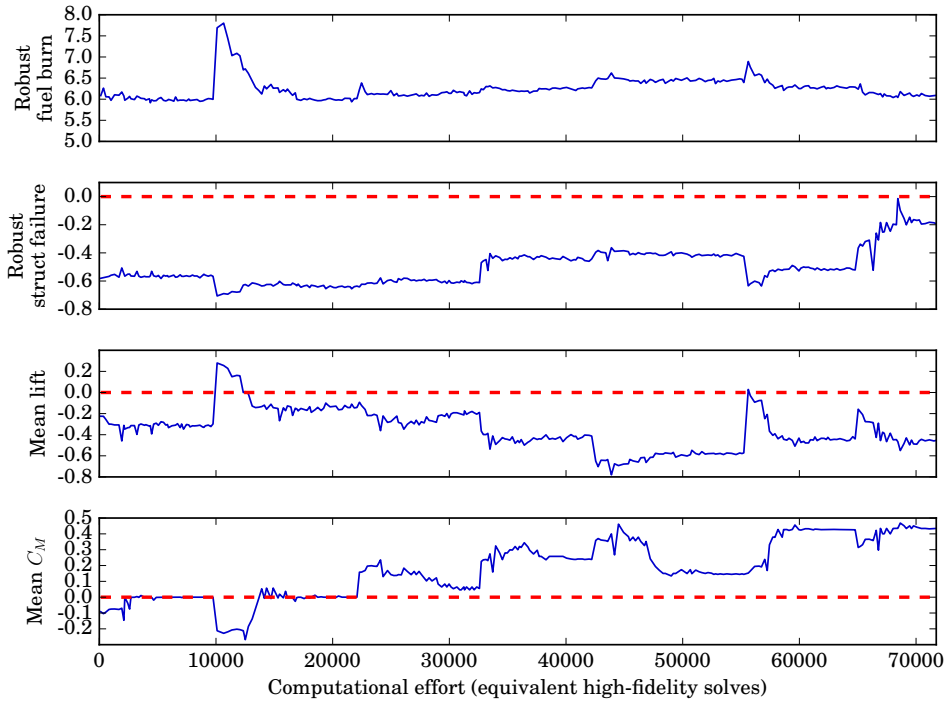

(a) Regular Monte Carlo

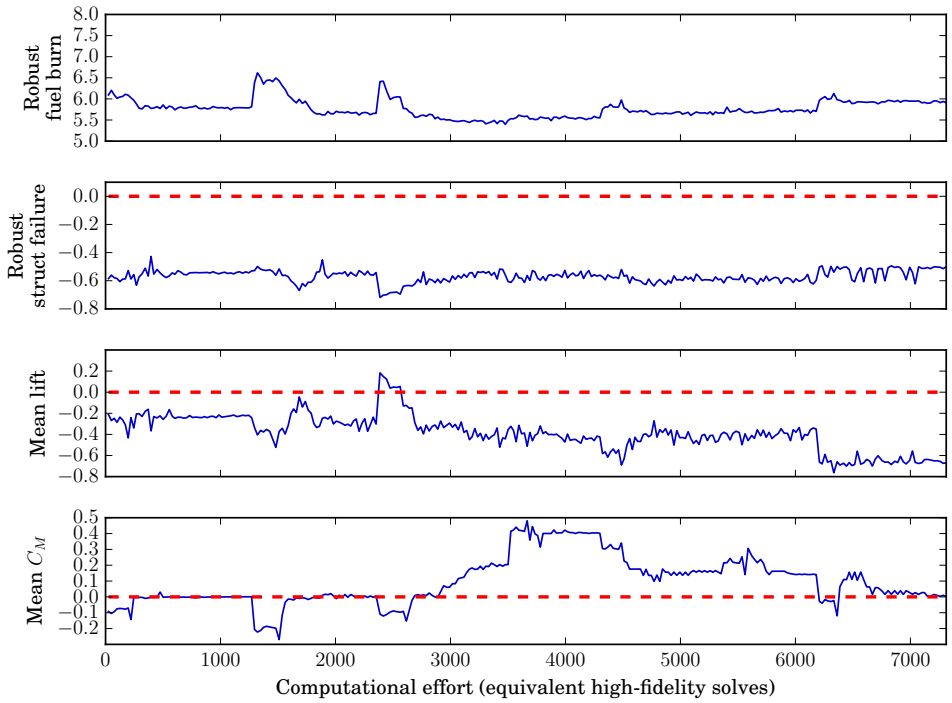

(b) Multifidelity

Fig. 10 Optimization history of the robust objective function and constraints for $\eta = 3$ associated with each visited design versus computational effort. Red dashed line shows the feasibility limit for the constraints. Note that the computational effort on the x-axis of the two plots have different magnitudes.

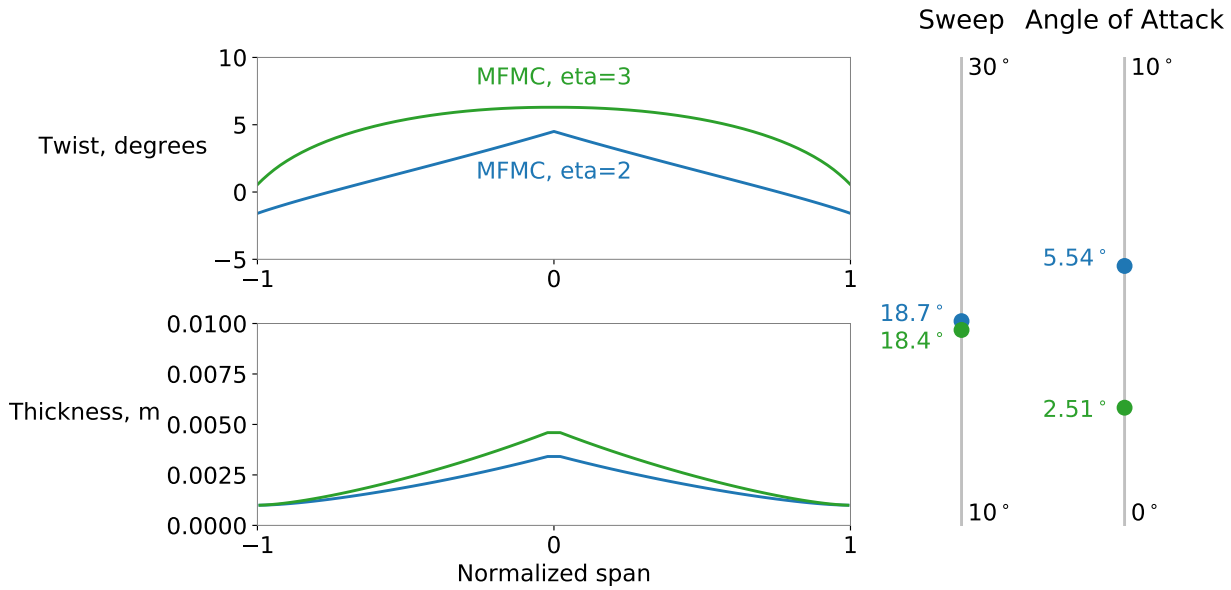

Fig. 11 Comparison of the best designs obtained via MFMC for $\eta = 2$ and $\eta = 3$. The spar thickness is greater and the twist distribution varies more smoothly for the $\eta = 3$ case.